

The physical and electrochemical properties of poly(vinylidene chloride-co-acrylonitrile)-based polymer electrolytes prepared with different plasticizers

C. Subbu^{1,2} · S. Rajendran¹ · K. Kesavan¹ · R. Premila¹

Received: 27 April 2015 / Revised: 30 July 2015 / Accepted: 10 August 2015 / Published online: 4 September 2015
© Springer-Verlag Berlin Heidelberg 2015

Abstract Lithium ion-conducting membranes with poly(ethylene oxide) (PEO)/poly(vinylidene chloride-co-acrylonitrile) (PVdC-co-AN)/lithium perchlorate (LiClO_4) were prepared by solution casting method. Different plasticizers ethylene carbonate (EC), propylene carbonate (PC), gamma butyrolactone (gBL), diethyl carbonate (DEC), dimethyl carbonate (DMC), and dibutyl phthalate (DBP) were complexed with the fixed ratio of PEO/PVdC-co-AN/ LiClO_4 . The preparation and physical and electrochemical properties of the gel polymer electrolytes have been briefly elucidated in this paper. The maximum ionic conductivity value computed from the ac impedance spectroscopy is found to be $3 \times 10^{-4} \text{ S cm}^{-1}$ for the EC-based system. From DBP-based system down to EC-based system, a decrease of crystallinity and an increase of amorphousness are depicted by X-ray diffraction technique, the decrease of band gap energy is picturized through UV–visible analysis, the decrease of glass transition temperature is perceived from differential scanning calorimetry plots, and the reduction of photoluminescence intensity is described through photoluminescence spectroscopy study at an excitation wavelength of 280 nm. Atomic force microscopic images of EC-based polymer electrolyte film show the escalation of micropores. Fourier transform infrared spectroscopy study supports the complex formation and the interaction between the polymers, salt, and plasticizer. The maximum thermal stability is obtained from thermogravimetry/differential thermal analysis,

which is found to be 222 °C for the sample complexed with EC. The cyclic voltogram of the sample having a maximum ionic conductivity shows a small redox current at the anode, and cathode and the chemical stability is confirmed by linear sweep voltammetry.

Keywords Ionic transport · Complex formation · Free anion · Polymer chain · Fluorescence intensity

Introduction

Since the polymer electrolytes are capable of providing a higher output voltage, higher specific heat capacity, long cycle life, improved safety, and so on, their applications for Li secondary are very wide and outstanding. Hence, the studies on polymer electrolytes have reasonably increased in the recent decades [1–3]. The first polymer-based solid polymer electrolyte was suggested by Armand et al. [4]. Subsequently, the solid polymer electrolytes were considered for an ideal alternate to the liquid electrolytes. Starting from 1970, poly(ethylene oxide) (PEO) and alkali metal salt-based solid polymer electrolytes got great consideration [5–7]. However, their ionic conductivity at ambient temperature is very low and is yet scarcely used for practical applications at elevated current densities. Many attempts have been made to increase the room temperature ionic conductivity in the polymer matrix. These attempts include innovative polymer synthesis [8–10], cross-linking of two polymers [11–13], blending of two polymers [14, 15], formulation of plasticized polymer electrolytes [16–18], synthesis of composite polymer electrolytes by the addition of inorganic fillers [19–21], and the formation of porous electrolytes employing the phase inversion method [22–24].

✉ S. Rajendran
sraj54@yahoo.com

¹ School of Physics, Alagappa University,
Karaikudi, Tamilnadu 630004, India

² Alagappa Government Arts College, Karaikudi, Tamilnadu 630003,
India

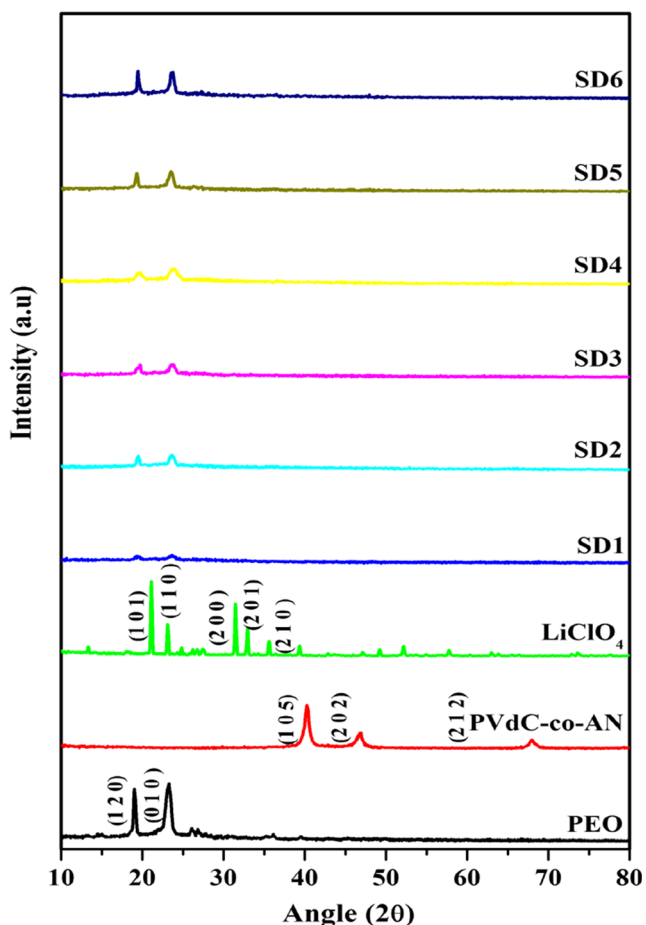


Fig. 1 XRD patterns of the pure and prepared samples

Out of these above mentioned techniques, blending of another polymer with PEO has been identified to have a good compatibility. Blending can, however, have profound and sometimes unexpected effects on thermal stability, which cannot simply be predicted on the basis of the behavior of the components and their relative properties [25]. A common approach is to add low molecular weight plasticizers to the polymer electrolytes [7]. The plasticizers impart salt solvating power and high ion mobility to the polymer electrolytes. PEO is the most interesting base material because of its high chemical and thermal stability. It can solvate a wide variety of salts even at high concentrations [26].

On the other hand, the addition of vinylidene chloride unit with poly(acrylonitrile) (PAN) gives high mechanical stability. The ionic conductivity of PAN-based electrolytes is of the order of 10^{-5} – 10^{-6} S cm^{-1} with good thermal stability. PEO–oligomers with poly(vinylidene chloride-co-acrylonitrile)-based electrolytes were prepared by Kim et al. [27]. They reported the conductivity of the order of 10^{-4} – 10^{-5} S cm^{-1} . In this work, we have chosen PVdC-co-AN as other polymer, because its mechanical and thermal stabilities are superior to other polymers.

Moreover, the ionic conductivity is an inherent property of high amorphousness and low viscosity. Since the viscosity of PEO is comparatively higher than that of PVdC-co-AN, the blending of PVdC-co-AN improves the ionic conductivity in addition to the enhancement of thermal and electrochemical stabilities. Barring that, to the best of the author's knowledge, a very little work has been carried out with PVdC-co-AN in the field of polymer electrolytes. Hence, an attempt has been made to synthesize new polymer blend electrolyte which could find applications in rechargeable lithium batteries.

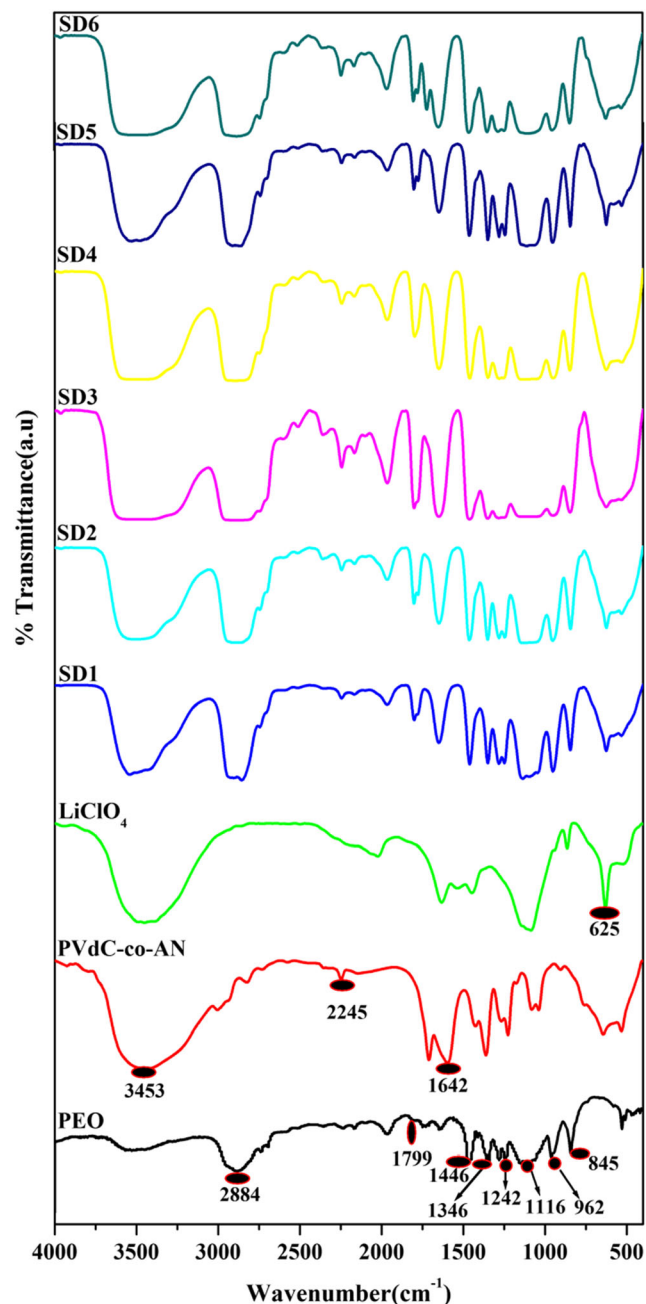


Fig. 2 FTIR spectra of the pure and the prepared samples

The present work explains the gel polymer electrolytes based on PEO/PVdC-co-AN/LiClO₄ complex by the addition of different plasticizers using a well-known solvent casting technique. The cyclability and reversibility of the prepared electrolytes have been studied. The ionic conductivity at different temperatures of the gel electrolytes has also been reported.

Materials and methods

The solution casting technique was used to prepare the gel polymer electrolyte films. Poly(ethylene oxide) $M_w \sim 8,000$, poly(vinylidene chloride-co-acrylonitrile) $M_w \sim 150,000$, and LiClO₄ were purchased from Sigma-Aldrich Chemicals Limited, USA, and they were used as received. PEO and PVdC-co-AN were dried at 50 °C under vacuum for 4 h to remove moisture. The salt was annealed at 60 °C under vacuum for 24 h. The plasticizers were also procured from Sigma-Aldrich, USA. The solvent tetrahydrofuran (THF) was acquired from E-Merck. Different gel polymer electrolytes were prepared with a constant ratio of PEO (64 wt%)/PVdC-co-AN (16 wt%)/LiClO₄ (8 wt%)/X (12 wt%) (where X = EC, PC, gBL, DEC, DMC, and DBP). The polymers, salt, and plasticizer were dissolved separately and mixed together. The mixed solution was stirred for 24 h with the help of a magnetic stirrer to obtain a homogeneous mixture. The solvent THF in the solution was allowed to evaporate slowly. Finally, the homogeneous solution was cast on Petri dishes. The Petri dishes containing the solution were dried at 50 °C under vacuum for 12 h to remove the residual solvent. The resulting free standing films were smoothly removed from the Petri dishes and

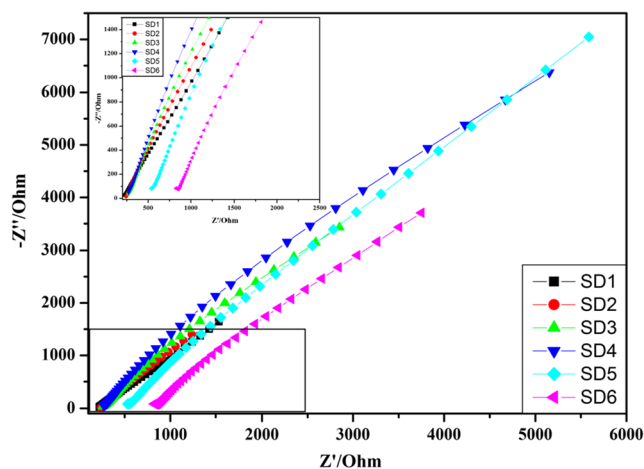


Fig. 3 Room temperature complex impedance plots of the prepared samples

cut into required shapes. The thickness of the harvested films was in the order of about 0.3–0.4 mm.

The X'Pert PRO PANalytical X-ray diffractometer was used to do the structural analysis of the films at room temperature. The complex formation between the polymer complex and salt was ratified by SPECTRA RXI, PerkinElmer spectrophotometer in the range 400–4,000 cm⁻¹. The ionic conductivity studies were carried out by placing the electrolyte film between the stainless steel blocking electrodes using a computer-controlled micro Autolab type III Potentiostat/Galvanostat in the frequency range 100 Hz–300 KHz. PerkinElmer PYRIS DIAMOND Thermogravimetry/Differential Thermal Analyzer (TG/DTA) was used to study the thermal stability of the blends from room temperature to 750 °C at a scan rate of 10 °C min⁻¹. Mettler Toledo differential scanning calorimetry (DSC) (822e) instrument was

Table 1 Assignments of FTIR absorption bands for the prepared membranes

Band assignment	Wave number (cm ⁻¹)							
	PEO	PVdC-co-AN	SD1	SD2	SD3	SD4	SD5	SD6
–OH group vibration	–	3,445	3,454	3,451	3,454	3,455	3,448	3,452
–CH ₂ sym stretching	2,884	–	2,889	2,891	2,880	2,883	2,891	2,887
C≡N stretching	–	2,245	2,245	2,244	2,251	2,255	2,244	2,240
Ether oxygen group	1,799	–	1,797	1,804	1,797	1,797	1,806	1,802
C=N stretching	–	1,642	1,646	1,648	1,646	1,653	1,653	1,646
–CH ₂ scissoring	1,468	–	1,460	1,462	1,462	1,460	1,463	1,462
–CH ₂ wagging	1,346	–	1,356	1,352	1,359	1,354	1,350	1,351
–CH ₂ twisting	1,242	–	1,254	1,249	1,249	1,247	1,242	1,240
C–O–C asymmetrical stretching	1,116	–	1,111	1,100	1,098	1,109	1,107	1,107
CH ₂ symmetrical rocking	962	–	964	955	949	964	955	955
–CH ₂ rocking	845	–	837	848	846	852	854	854
ClO ₄ ⁻ anion	–	–	627	635	627	629	629	635

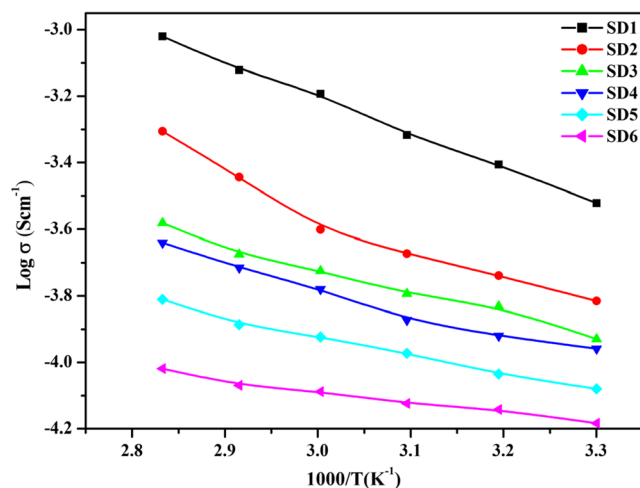


Fig. 4 Temperature dependent ionic conductivity plots of the prepared samples

employed to study the phase changes using differential scanning calorimetry. Using Cary Eclipse Fluorescence Spectrometer, the photoluminescence studies of the films were carried out. UV–visible analysis of the prepared films was done with (Lambda 35) PerkinElmer UV–visible spectrometer to calculate the optical band gap of the complexes. The surface morphology of the film having a maximum ionic conductivity was studied by JEOL, JSM-840A. AFM (A100SGS) was used to study the complex film having a maximum ionic conductivity. Computer-controlled micro Autolab type III potentiostat/galvanostat was employed for cyclic voltammetry and linear sweep voltammetry studies.

Results and discussion

X-ray diffraction analysis

Figure 1 delineates X-ray diffraction peaks of pure PEO, PVdC-co-AN, LiClO₄, and prepared gel polymer electrolytes. The sharp, intense peaks at $2\theta=19.1$ and 23.3° associated with the lattice planes (1 2 0) and (0 1 0) signify the semi-crystalline

nature of PEO. The crystalline nature of PVdC-co-AN is affirmed by the diffraction angles at $2\theta=40.25^\circ$, 46.76° , and 67.94° compatible to (1 0 5), (2 0 2), and (2 1 2) lattice planes. The strong crystallinity of LiClO₄ and BaTiO₃ is discerned from the diffraction angles at $2\theta=18.36^\circ$, 23.2° , 27.5° , 32.99° , and 36.58° and 22° , 31° , 45° , 51° , 56° , 65° , 70° , and 75° pertaining to the lattice planes (1 0 1), (1 1 0), (2 0 0), (2 0 1), and (2 1 0) and (1 0 0), (1 1 0), (1 1 1), (2 0 0), (2 1 0), (2 1 1), (2 2 0), and (3 0 1), respectively.

From Fig. 1, it is observed that with the addition of lithium salt and different plasticizers to the polymer blend, the intensity of these peaks decreases gradually. These observations apparently reveal that the polymer blend undergoes significant structural reorganization upon the addition of different plasticizers. The plasticizers might have induced significant disorder into the original polymers, and this is attributed to the interactions between polymer and the solvents, which resulted in polymer electrolytes with much lower crystallinity. Hence, the absence of peaks pertaining to lithium perchlorate salt in the complexes indicates the complete dissolution of the salt in the polymer matrix.

FTIR studies

Fourier transform infrared spectroscopy (FTIR) is a quite commonly used technique to examine the interactions in polymer blends [28, 29]. The immiscibility and the phase separation between the blending components will be identified by the spectra of pure individual components. On the other hand, the miscibility of the components is implied by the possibility of chemical interactions between the individual polymer chains, salt, and plasticizer. Generally, wave number shifts, increase or decrease in the intensity of the peaks, and broadening are taken as evidence of chemical interactions between the components in a blend and are indicative of miscibility.

Figure 2 illustrates the FTIR spectra of pure PEO, PVdC-co-AN, and salt and those of the prepared sample with different plasticizers, and Table 1 shows the various band assignments corresponding to the wave numbers. The broad vibrational peak around $3,445\text{ cm}^{-1}$ in the spectra pertaining to the

Table 2 Ionic conductivity values of the prepared samples

Sample code	Composition of the prepared samples in wt%	Conductivity values for different temperatures (σ) $\times 10^{-4}\text{ S cm}^{-1}$					
		303 K	313 K	323 K	333 K	343 K	353 K
SD1	X = EC	3.0	3.92	4.82	6.42	7.56	9.55
SD2	X = PC	1.53	1.83	2.12	2.5	3.6	4.95
SD3	X = gBL	1.18	1.47	1.61	1.88	2.11	2.62
SD4	X = DEC	1.1	1.2	1.34	1.66	1.93	2.29
SD5	X = DMC	0.83	0.922	1.06	1.19	1.3	1.55
SD6	X = DBP	0.66	0.72	0.75	0.83	0.85	0.96

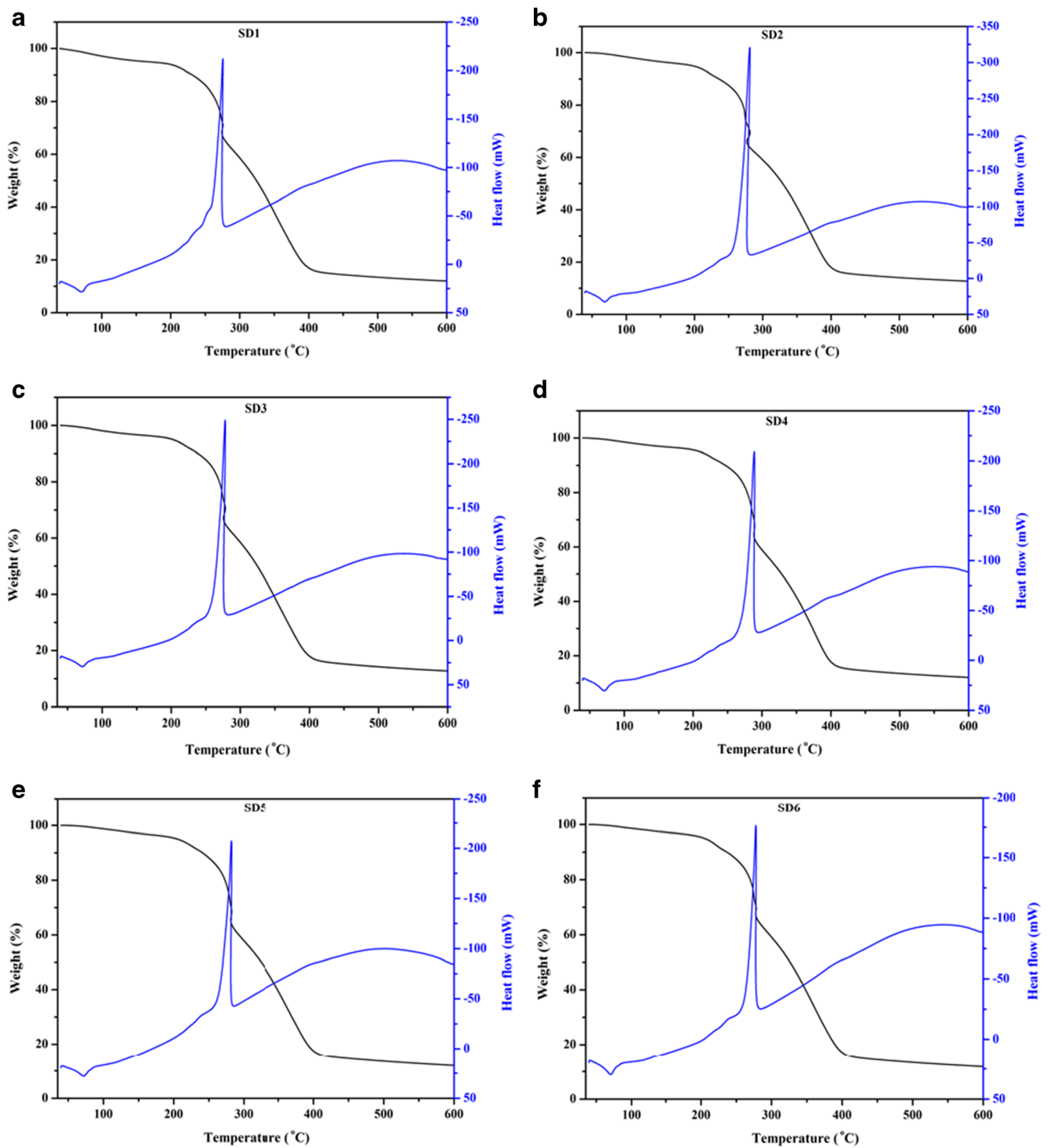


Fig. 5 a–f TG/DTA plots of the prepared blend electrolytes

–OH group [30] is attributed to the water or moisture absorption which might have happened during the sample loading for the spectral analysis. The peak $3,445\text{ cm}^{-1}$ is shifted to the wave numbers $3,454, 3,451, 3,454, 3,455, 3,448,$ and $3,452\text{ cm}^{-1}$ in all the prepared complexes. The well-built vibrations of $\text{C}\equiv\text{N}$ and $\text{C}=\text{N}$ bands in PVdC-co-AN [30] are represented by the peaks around $2,245$ and $1,642\text{ cm}^{-1}$. These two

peaks are shifted to the wave numbers $2,244, 2,251, 2,255, 2,244,$ and $2,240\text{ cm}^{-1}$ and $1,646, 1,648, 1,646, 1,653,$ and $1,646\text{ cm}^{-1}$, respectively, in the EC-, PC-, gBL-, DEC-, DMC-, and DBP-based gel polymer electrolytes.

The symmetric and asymmetric C–H stretching forms of CH_2 in PEO [31] is symbolized by the strong absorption band appearing around $2,800\text{--}2,950\text{ cm}^{-1}$ which shifts in the wave

Table 3 TG/DTA results of the prepared samples

Sample code	Decomposition temperature (°C)			Weight loss of the samples in %			Exothermic peaks (°C)		
	I	II	III	I	II	III	I	II	III
SD1	88	272	395	3	33	82	71	274	391
SD2	80	278	404	2	35	83	67	282	399
SD3	77	276	405	2	35	83	71	279	397
SD4	77	289	404	3	38	83	71	289	395
SD5	75	282	400	2	37	83	72	282	395
SD6	73	275	403	2	34	84	69	276	386

numbers 2,889, 2,891, 2,880, 2,883, 2,891, and 2,887 cm^{-1} in all the prepared electrolytes. The strong vibration of the ether oxygen group in PEO is indicated by the peak around 1,799 cm^{-1} [32] which is shifted to the wave numbers 1,797, 1,804, 1,797, 1,797, 1,806, and 1,802 cm^{-1} . A strong vibrational peak at 1,468 cm^{-1} is attributed to CH_2 stretching of pure PEO which is shifted to 1,460, 1,462, 1,462, 1,460, 1,463, and 1,462 cm^{-1} , respectively [33]. It can be seen that the CH_2 asymmetric wagging mode appearing at 1,346 cm^{-1} for pure PEO shifts to the wave numbers 1,356, 1,352, 1,359, 1,354, 1,350, and 1,351 cm^{-1} , respectively [34]. The $-\text{CH}_2$ symmetric twisting mode is embodied by the peak near 1,242 cm^{-1} in pure PEO which has been shifted to the wave numbers 1,254, 1,249, 1,249, 1,247, 1,242, and 1,240 cm^{-1} in the samples SD1, SD2, SD3, SD4, SD5, and SD6, respectively [34]. The peak relating to the antisymmetric stretching vibration of the C–O–C bridge in PEO becomes visible close to 1,116 cm^{-1} [35], and it is shifted in the complexes to the wave numbers 1,111, 1,100, 1,098, 1,109, 1,107, and 1,107 cm^{-1} , respectively. The peak corresponding to ClO_4^- vibration is found around 625 cm^{-1} which is present in all the complexes.

New peaks pertaining to the absorption at 2,166, 1,965, and 1,460 cm^{-1} of EC-based complex, 2,744, 2,359, 2,165, 1,965, 1,462, and 1,245 cm^{-1} of PC-based complex, 2,511, 2,358, and 1,964 cm^{-1} of gBL-based complex, 2,513, 2,353, and 2,167 cm^{-1} of DEC-based complex, 2,742, 2,361, and 1,244 cm^{-1} of DMC-based complex, and 2,743, 2,165, and 1,720 cm^{-1} of DBP-based complex are also present in the FTIR spectra of the complexes.

The disappearance of the few characteristic peaks of the plasticizers and the appearance of the new peaks and shift in the peaks confirm the complex formation between polymers, salt, and different plasticizers.

Complex impedance analysis

The conduction mechanism is studied with the help of ac impedance spectroscopy by observing the contribution of polymeric chain, mobility, and carrier generation process [36]. Figure 3 depicts the room temperature ionic conductivity of the prepared gel polymer electrolytes. The theoretical analysis given by Watanabe and Ogata [37] stipulates for two

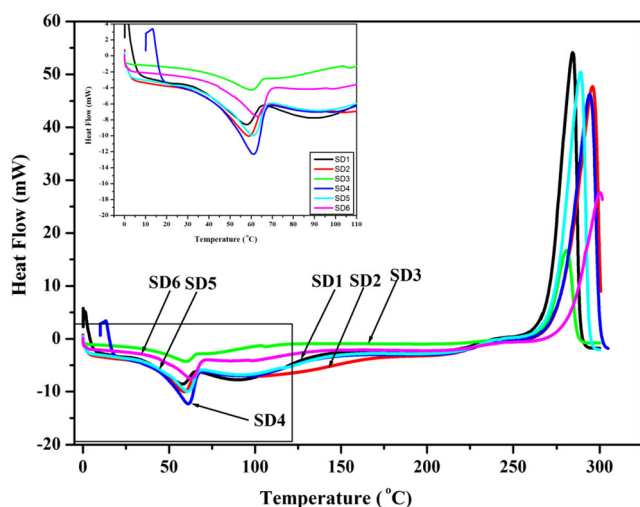
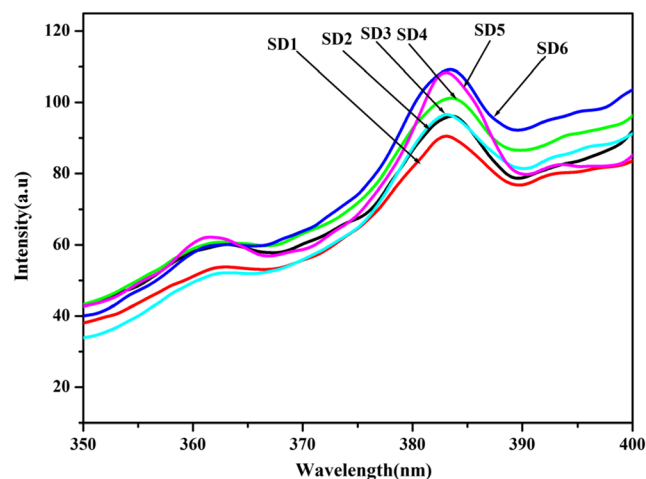
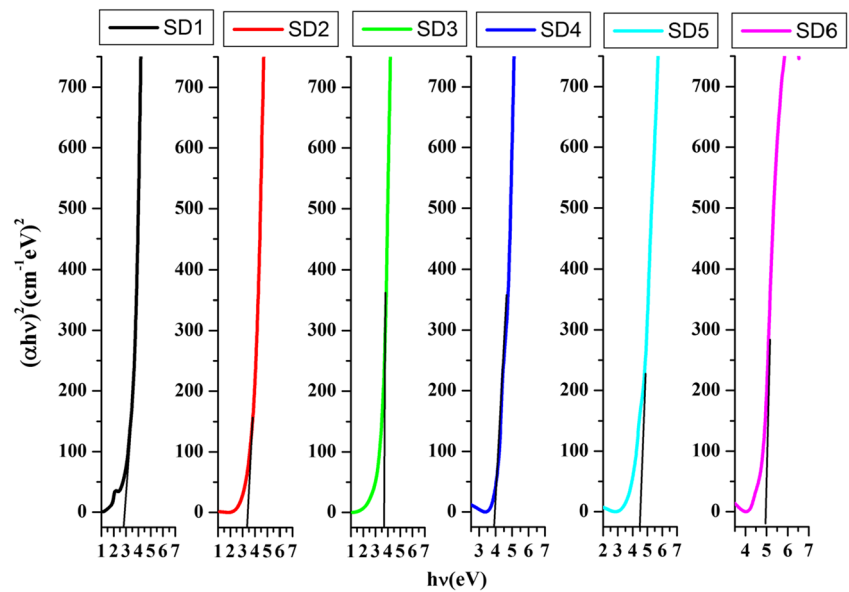
**Fig. 6** DSC curves of the prepared polymer electrolytes**Fig. 7** Photoluminescence spectra of the prepared complexes

Fig. 8 Plots for direct band gap of the prepared samples



semicircles to be present in the impedance spectrum of asymmetric cell. One semicircle at high-frequency region embodies the bulk electrolyte impedance, and the other at low-frequency region corresponds to the interfacial impedance. Reports say that the high frequency semicircles will not appear in the practical impedance plots of plasticized polymer electrolyte membranes [38, 39]. This feature reveals that the conductivity in these films is established mainly by the ions and which is calculated using the formula $\sigma=l/(R_b \cdot A)$, where A is the area of the film surface in contact with the electrodes, l is the thickness of the film, and the value of bulk resistance (R_b) is taken on the X -intercept of the impedance plots. The film SD1 complexed with EC plasticizer is found to have maximum

ionic conductivity value of $3 \times 10^{-4} \text{ S cm}^{-1}$ at 303 K. The rationale is clarified as follows.

In general, the influence of plasticizer in the ionic conductivity of the polymer electrolyte films is determined by its own characteristics like dielectric constants, viscosity, polymer–plasticizer interaction, and ion–plasticizer interaction. In this view, the plasticizer EC possesses a high dielectric constant (89 at 40 °C) and comparatively low viscosity (1.9 cP). This may be the reason for the high ionic conductivity of the film SD1 complexed with EC. The plasticizers would dissolve enough charge carriers and provide more mobile medium for the ions so as to enhance the conducting behavior of the samples [40]. The conductivity is obtained in the decreasing order

Fig. 9 Plots for indirect band gap of the prepared samples

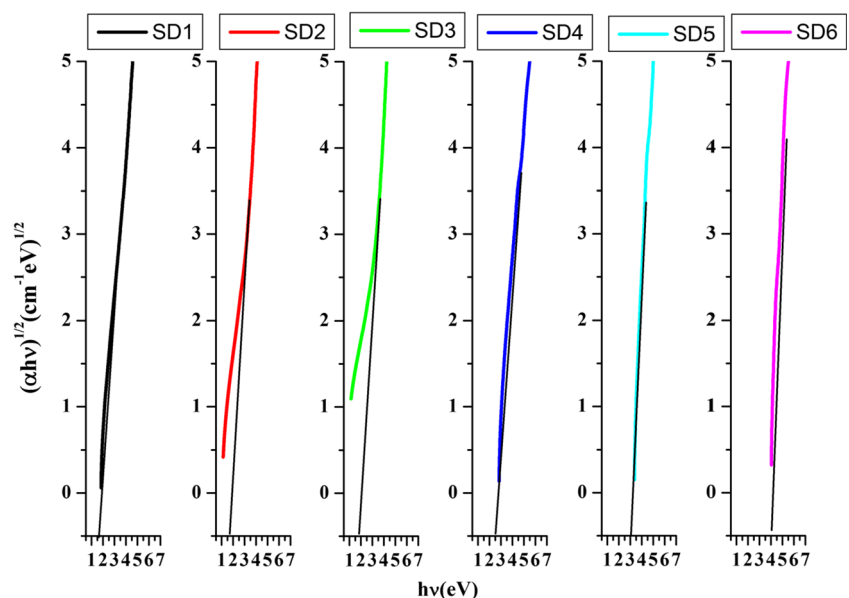


Table 4 Direct and indirect band gap values of the prepared complexes

Sample code	Band gap values in eV	
	Direct	Indirect
SD1	2.8	1.6
SD2	3.4	1.8
SD3	3.7	2.0
SD4	3.9	2.6
SD5	4.5	3.2
SD6	5.0	4.0

of the EC-, PC-, gBL-, DEC-, DMC-, and DBP-based gel polymer electrolytes which are in accordance with their dielectric constants 90, 64, 42, 28, 11, and 8.4, respectively. These results agree well with the earlier reports using different plasticizers [41, 42].

The ionic conductivity values of the sample observed over the temperature range 303–363 K have been plotted in Fig. 4. It could be visualized that the conductivity values increase with the increase of temperature regardless the nature of the sample as given in Table 2. This enhancement in the conductivity values with increase of temperature could be elucidated with the free volume theory [43]. Free volume is produced when the polymer expands with temperature and the polymer segments or molecules solvated with ions can move spasmodically into the free volume. The free volume around the polymer chain decides the overall mobility of the ions and the polymer segment, which represents the resultant ionic conductivity of the films. Hence, the ionic mobility and segmental mobility gear up the ion transport by overcoming the retarding effects of the ion clouds. The plot of the temperature-dependent ionic conductivity indicates that the ion conduction in the solid polymer electrolytes seems to obey the Vogel-Tammann-Fulcher (VTF) relation which describes the transport mechanism in a viscous matrix [44–47].

TG/DTA

All the physical phenomena associated with the weight changes are elaborately studied using TG/TDA. TG/DTA curves of EC-, PC-, gBL-, DEC-, DMC-, and DBP-based PEO/PVdC-co-AN/LiClO₄ systems have been plotted as shown in Fig. 5(a–f).

Table 3 illustrates weight changes with temperature. It is seen from Fig. 5 that the initial weight loss about 2–3 % is observed in the temperature range 76–88 °C. This may be due to the removal of residual solvent and moisture if any. The second weight losses attributing to the structural changes in the polymers occur between 272 and 289 °C which are 33, 35, 35, 38, 37, and 34 % for the samples SD1, SD2, SD3, SD4, SD5, and SD6,

respectively. Then, there is no appreciable weight loss observed until the temperature reaches around 395–405 °C. Maximum thermal stability 222 °C is observed for the sample SD1.

The DTA plots of the samples exhibit endothermic peaks between 67 and 71 °C. The second and third peaks are exothermic peaks in the range of 274–289 and 386–395 °C, respectively, which are well correlated with the weight loss of all the samples observed in TG curve.

DSC analysis

This technique is used to measure the difference in heat flow rate between the sample and inert reference as a function of time and temperature. The processes like glass transition, melting, evaporation, etc. are associated with the endothermic heat flow, whereas the physical events like crystallization, cure, oxidation, etc. are accompanied by an exothermic heat flow.

Figure 6 displays the DSC plots of the samples with various plasticizers. It is noticed that the samples SD1, SD2, SD3,

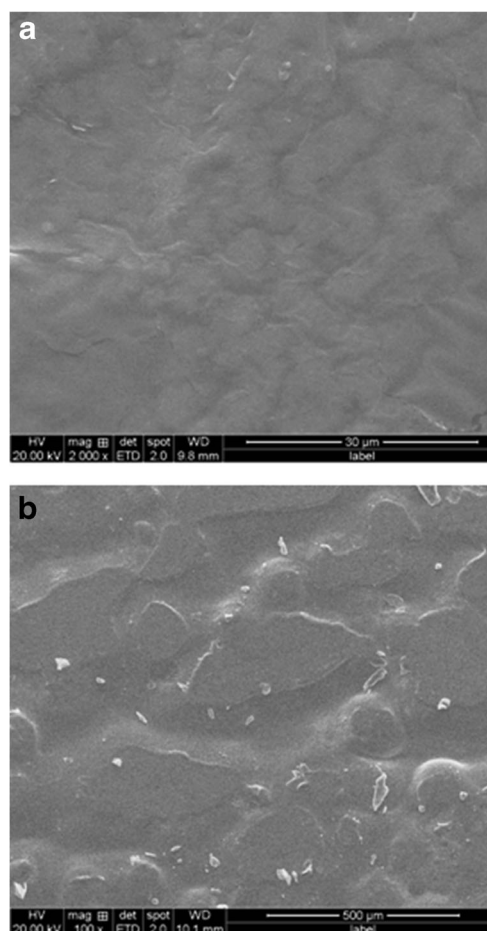


Fig. 10 SEM analysis of the sample (SD1) having a maximum ionic conductivity at different magnifications. **a** $\times 2,000$. **b** $\times 100$

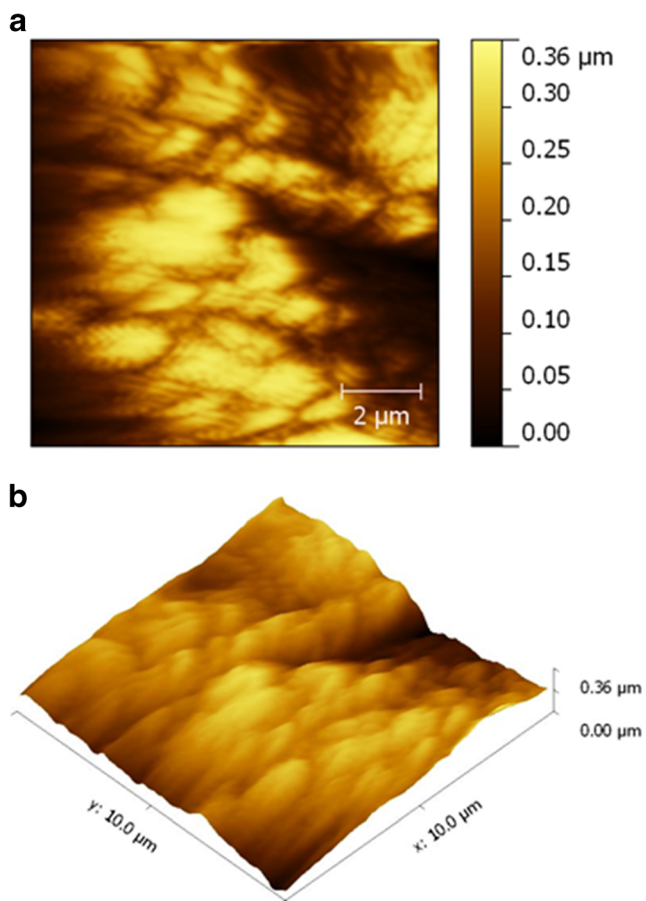
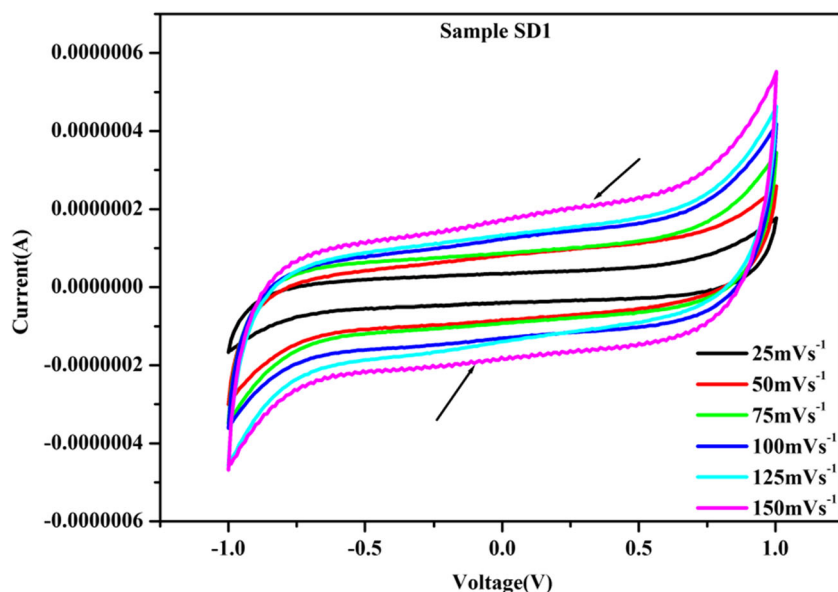


Fig. 11 The topographic image of the sample (SD1) having a maximum ionic conductivity. **a** Two-dimensional image. **b** Three-dimensional image

SD4, SD5, and SD6 show a phase transition at 27, 28, 30, 31, 32, and 33 °C which are ascribed to the glass transition temperatures of the prepared complexes accordingly. The glass

Fig. 12 Cyclic voltammograms of the sample having a maximum ionic conductivity (SD1)



transition temperature of PEO is -53 to -45 °C and that of PVdC-co-AN is around 50 °C. Among the different complexes, the sample prepared with EC shows a minimum T_g value which attributes to its maximum ionic conductivity. The decrease in the T_g value also indicates the decrease of crystallinity upon the addition of plasticizer.

Photoluminescence studies

The polymer electrolyte films prepared with various plasticizers were subjected to photoluminescence analysis at an excitation wavelength of 280 nm. Figure 7 shows photoluminescence emission spectra of the prepared electrolytes. The carrier mobility of the electrolyte is inversely proportional to the local viscosity. But the local viscosity is directly associated with the emission intensity [48, 49].

In the present study, EC-based polymer electrolyte system has a minimum emission intensity as compared to other samples. This might be due to the maximum dissociation of the ionic charge carriers owing to its high dielectric constant. As the photoluminescence emission intensity decreases, the local viscosity of the surrounding polymeric media also decreases. This in turn increases the ionic mobility and hence conductivity. These results are exclusively concurring with the ionic conductivity values (Table 2).

UV-visible analysis

The optical absorption study of the polymer electrolyte films provides the band structure details of the solids. Generally, insulators and semiconductors are categorized into direct band gap materials and indirect band gap materials. Direct band gap materials are identified with

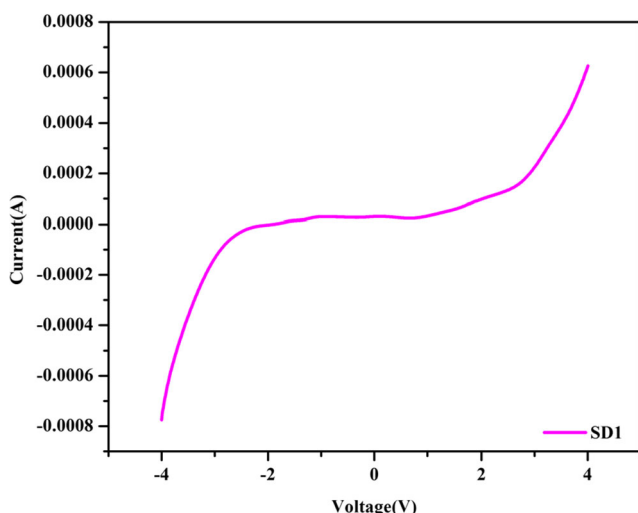


Fig. 13 Linear sweep voltammetric plot of the sample having a maximum ionic conductivity (SD1)

the zero crystal momentum associated with the top of the valence band and the bottom of the conduction band. But, the bottom of the conduction band possesses non-zero crystal momentum in the case of indirect band gap materials.

In indirect band gap materials, a photon of the light magnitude of crystal momentum is associated with the transition from the valence band to the conduction band. The band gap of the materials is determined by the knowledge of the fundamental absorption pertaining to the transition from the valence band to the conduction band.

The energy of the incident photon ($h\nu$) and the absorption co-efficient α are related by the following expression

$$\alpha = C \left[\frac{(h\nu - E_g)^n}{h\nu} \right]$$

where C is a constant and E_g is the band gap of the materials. The type of transition is determined by the exponent which assigns the values 1/2 for direct and 2 for indirect and for forbidden direct and forbidden indirect transitions, respectively [50].

The calculated values of $(\alpha h\nu)^2$ and $(\alpha h\nu)^{1/2}$ were plotted against $h\nu$ separately for all the samples as shown in Figs. 8 and 9, respectively. The direct band gap value was evaluated from $(\alpha h\nu)^2$ vs $h\nu$ by extrapolating the linear portions of the curves to zero absorption. For the sample SD1, the direct band gap lies at 2.8 eV, while for the samples SD2, SD3, SD4, SD5, and SD6, they lie at 3.4, 3.7, 3.9, 4.5, and 5.0 eV, respectively. On the other hand, the indirect band gap values were obtained from plots of $(\alpha h\nu)^{1/2}$ vs $h\nu$ at the intercepts of the energy axis on extrapolating the linear portion of the curve to zero absorption value (Fig. 9). The indirect band gap value of the sample SD1, SD2, SD3, SD4, SD5, and SD6 are 1.6, 1.8, 2.0, 2.6, 3.2, and 4.0 eV, respectively.

The direct and indirect band gap values have been displayed in Table 4. EC plasticizer-based gel polymer electrolyte is found to have a minimum band gap as compared to other plasticizer-based samples. However, all the complexes prepared with different plasticizers show a significant decrease in the band gap values for direct and indirect band gap calculations. This may be due to the formation of defects in the electrolytes which produce localized states in the optical band gap, and these states are accountable for the decrease in energy band gaps [51]. These results are in agreement with those obtained from conductivity studies.

Scanning electron microscopic study

Scanning electron microscope was employed to study the surface morphology of the film SD1 with maximum ionic conductivity. Figure 10(a, b) displays the surface morphology of the film with two different magnifications $\times 2,000$ and $\times 100$. It is observed that the addition of plasticizer has considerably reduced the roughness of the film. The smooth and homogeneous surface morphology indicates a remarkable increase in the amorphousness which is responsible for the increase in ionic conductivity of this film. This result is in good agreement with the X-ray diffraction and conductivity studies.

Atomic force microscopic analysis

The atomic force microscope was used to study the two- and three-dimensional topographical images of the sample having a maximum ionic conductivity. Figure 11(a, b) represents the topographic images. From the figures, we are able to understand that there are number of pores within the scanned area of $50 \times 50 \mu\text{m}$. These small pores of the electrolyte are responsible for the enhancement of ionic conductivity. The pores helped to ensnare the large volume of the liquid in the pores accounting for the increased conductivity. The rms roughness value is found to be 200.9 nm. The increase of pore size and smoothness might be the rationale for the increased ionic conductivity of this film which agrees with the ionic conductivity results.

Cyclic voltammetric test

Since high ionic conductivity is not a sufficient property to make an electrolyte useful in practical terms, the electrochemical stability of the gel polymer electrolyte film (SD1) (PEO (64 wt%)/PVdC-co-AN (16 wt%)/LiClO₄ (8 wt%)/EC (12 wt%)) exhibiting maximum ionic conductivity was explored using cyclic voltammetry. The cyclic voltammograms of the SS/gel polymer electrolyte/SS cell couple was taken at different scan rates (25–150 mV/s) as shown in Fig. 12. There is one poorly defined anodic peak around 0.28 V and one less prominent cathodic peak near

–0.09 V. This may be due to the strong capacitive current [52]. These peaks are associated with the oxidation and reduction of $\text{LiClO}_4/\text{polymer}$ at the anode and cathode, respectively.

It is also noticed that the area of the rectangles increases with the increase of scan rates. This reveals that the voltammetric current is directly proportional to the scan rate. The poor rectangular shape with the higher scan rate could be explained that the ion species from the polymer film may confront the difficulty to enter all the vacant sites in the active electrode. This pertains to the partial rate of movement in the electrolyte [53]. The overall performance of the polymer electrolyte film as separator is highly capacitive and electrochemically reversible.

Liner sweep voltammetric test

The electrochemical stability window of the gel polymer electrolyte having a maximum ionic conductivity was determined by linear sweep voltammetry with a constant scan rate (50 mV/s) [54] as shown in Fig. 13. The decomposition process of the polymer electrolyte results in the onset of current in the anodic higher voltage range and cathodic low voltage range [55]. The stability window for this film is observed around –2.8 to +2.6 V and also indicates there is no decomposition of any component in this potential range.

Conclusion

The gel polymer electrolytes consisting of PEO/PVdC-co-AN/ LiClO_4 with different plasticizers were prepared by solution casting technique. The reduction in the XRD peaks and the increase of amorphousity due to the addition of plasticizers were confirmed by X-ray diffraction technique. The complex formation and the interaction between polymer-plasticizer and ion-plasticizer were ascertained by FTIR analysis. The ionic conductivities were calculated using ac impedance analysis. The maximum room temperature ionic conductivity value is found to be $3 \times 10^{-4} \text{ S cm}^{-1}$ for the film prepared with EC plasticizer owing to its high dielectric constant. The sample (SD1) has the highest ionic conductivity which is supported by the lowest optical band gap in UV–visible spectroscopy. The two- and three-dimensional topographic images of the sample having a maximum ionic conductivity show the presence of number of pores which are responsible for high ionic conduction. The maximum thermal stability is found to be 222 °C for the sample SD1. The emission peaks observed from the photoluminescence spectra were in line with the conductivity results. The CV results show a strong capacitive behavior, cyclability, and reversibility of the above gel polymer electrolyte. The electrochemical window has been

observed to be –2.8 to +2.6 V. Hence, these data suggest that the present electrolyte system is a worthy candidate for battery applications.

References

1. Croce F, Appetecchi GB, Persi L, Scrosati B (1998) Nanocomposite polymer electrolytes for lithium batteries. *Nature* 394:456–458
2. Scrosati B (2001) New approaches to developing lithium polymer batteries. *Chem Rec* 1:173–181
3. Wakihara M (2001) Recent developments in lithium ion batteries. *Mater Sci Eng R Reports* 33:109–134
4. Gray FM (1991) Solid polymer electrolytes—fundamentals and technological applications. VCH, New York
5. Fenton DE, Parker JM, Wright PV (1973) Complexes of alkali metal ions with poly(ethylene oxide). *Polymer* 14:589
6. Wright PV (1975) Electrical conductivity in ionic complexes of poly(ethylene oxide). *Brit Polym J* 7:319–327
7. Feuillade G, Perche P (1975) Ion-conductive macromolecular gels and membranes for solid lithium cells. *J Appl Electrochem* 5:63–69
8. Xu Q, Wan G (1993) Rechargeable $\text{Li/LiMn}_2\text{O}_4$ batteries with a polymeric solid electrolyte. *J Power Sources* 41:315–320
9. Selvaraj II, Chaklanobis S, Chadrasekhar V (1995) Conductivity studies on poly(methoxyethoxyethylmethacrylate)-lithium salt complexes. *J Electrochem Soc* 142:366–370
10. Huang B, Wang Z, Chen L, Xue R, Wang F (1996) The mechanism of lithium ion transport in polyacrylonitrile-based polymer electrolytes. *Solid State Ionics* 91:279–284
11. Wiecek KW, Florjanczyk Z, Stevens JR (1995) Composite polyether based solid electrolytes. *Electrochim Acta* 40:2251–2258
12. Maccallum JR, Smith MJ, Vincent CA (1981) The effects of radiation-induced crosslinking on the conductance of $\text{LiClO}_4/\text{PEO}$ electrolytes. *Solid State Ionics* 11:307–312
13. Watanabe M, Nagano S, Sanui K, Ogata N (1987) Structure-conductivity relationship in polymer electrolytes formed by network polymers from poly[dimethylsiloxane-g-poly(ethylene oxide)] and lithium perchlorate. *J Power Sources* 20:327–332
14. Inganäs O (1988) Electroactive polymer blends. *Brit Polym J* 20: 233–236
15. Kim DW, Park JK, Rhee HW (1996) Conductivity and thermal studies of solid polymer electrolytes prepared by blending poly(ethylene oxide), poly(oligo[oxyethylene]oxy sebacoyl) and lithium perchlorate. *Solid State Ionics* 83:49–56
16. Nagasubramanian G, Attia AI, Halpert G (1994) A polyacrylonitrile-based gelled electrolyte: electrochemical kinetic studies. *J Appl Electrochem* 24:298–302
17. Stallworth PE, Greenbaum SG, Croce F, Slane S, Salomon M (1995) Lithium-7 NMR and ionic conductivity studies of gel electrolytes based on poly(methylmethacrylate). *Electrochim Acta* 40: 2137–2141
18. Morales JLA (1997) Thermal and electrical characterization of plasticized polymer. *Solid State Ionics* 96:99–106
19. Fan L, Nan CW, Dang Z (2002) Effect of modified montmorillonites on the ionic conductivity of $(\text{PEO})_{16}\text{LiClO}_4$ electrolytes. *Electrochim Acta* 47:3541–3544
20. Croce F, Curini R, Martinelli A, Persi L, Ronchi F, Scrosati B (1999) Physical and chemical properties of nanocomposite polymer electrolytes. *J Phys Chem B* 103:10632–10638
21. Nann C-W (1993) Physics of inhomogeneous inorganic materials. *Prog Mater Sci* 37:1–116

22. Gozdz AS, Schmutz CN, Tarascon JM (1994) Rechargeable lithium intercalation battery with hybrid polymeric electrolyte, US patent 5296318A
23. Michot T, Nishimoto A, Watanabe M (2000) Electrochemical properties of polymer gel electrolytes based on poly(vinylidene fluoride) copolymer and homopolymer. *Electrochim Acta* 45:1347–1360
24. Shi Q, Yu M, Zhou X, Yan Y, Wan C (2002) Structure and performance of porous polymer electrolytes based on P(VDF-HFP) for lithium ion batteries. *J Power Sources* 103:286–292
25. Zulfiqar S, Ahmad S (1999) Thermal degradation of blends of PVC with polysiloxane—I. *Polym Degrad Stab* 65:243–247
26. KiranKumar K, Ravi M, Pavani Y, Bhavan S, Sharma AK, Narasimha Rao VVR (2011) Investigations on the effect of complexation of NaF salt with polymer blend (PEO/PVP) electrolytes on ionic conductivity and optical energy band gaps. *Physica B* 406:1706–1712
27. Shanthi M, Mathew CM, Ulaganathan M, Rajendran S (2013) FT-IR and DSC studies of poly(vinylidene chloride-co-acrylonitrile) complexed with LiBF_4 . *Spectrochim Acta A* 109:105–109
28. Painter PC, Coleman MM (1997) Fundamentals of polymer science: an introductory text. Technomic Publishing, Lancaster
29. Garton A (1992) Infrared spectroscopy of polymer blends, composites and surfaces. Carl Hanser Verlag, Munich
30. Krimm S, Liang CY (1956) Infrared spectra of high polymers. IV. Poly(vinyl chloride), poly(vinylidene chloride), and copolymers. *J Polym Sci* 22:95–112
31. Suthanthiraraj SA, Sheeba DJ (2007) Structural investigation on PEO-based polymer electrolytes dispersed with Al_2O_3 nanoparticles. *Ionics* 13:447–450
32. Papke BL (1982) Vibrational spectroscopic determination of structure and ion pairing in complexes of poly(ethylene oxide) with lithium salts. *J Electrochem Soc* 129:1434–1438
33. Rigas B, Morgellon S, Goldman IS, Wong PT (1990) Human colorectal cancers display abnormal Fourier-transform infrared spectra. *Proc Natl Acad Sci U S A* 87:8140–8144
34. Bertie JE, Othen DA (1973) On the assignment of the infrared spectrum of ethylene oxide. *Can J Chem* 51:1155–1158
35. Wen SJ, Richardson TJ, Ghantous DI, Striebel KA, Ross PN, Cairns EJ (1996) FTIR characterization of PEO+ $\text{LiN}(\text{CF}_3\text{SO}_2)_2$ electrolytes. *J Electroanal Chem* 408:113–118
36. Ostrovski D, Brodin A, Torell M, Appetecchi GB, Scrosati BJ (1998) Molecular and ionic interactions in polyacrylonitrile- and poly(methylmetacrylate)-based gel electrolytes. *J Chem Phys* 109:7618–7624
37. Watanabe M, Ogata N, MacCullum JR, Vincent CA (1987) Polymer electrolyte review, vol 1. Elsevier, New York
38. Sung HY, Wang YY, Wan CC (1998) Preparation and characterisation of poly(vinyl chloride-co-vinyl acetate)-based gel electrolytes for Li-ion batteries. *J Electrochem Soc* 145:1207–1211
39. Abraham KM, Alamgir M, Hoffinan DK (1995) Polymer electrolytes reinforced by Celgard membranes. *J Electrochem Soc* 142:683–687
40. Mark HF (1964) Encyclopedia of polymer science and engineering, vol 1. Wiley Interscience Publication, John Wiley & Sons, New York
41. Ulaganathan M, Rajendran S (2010) Li ion conduction on plasticizer-added PVAc-based hybrid polymer electrolytes. *Ionics* 16:667–672
42. Mathew CM, Kesavan K, Rajendran S (2014) Analysis of plasticizer influence in poly(vinyl acetate)/poly(vinylidene fluoride) polymer blend electrolyte. *Ionics* 20:439–443
43. Miyamoto T, Shibayama K (1973) Free-volume model for ionic conductivity in polymers. *J Appl Phys* 44:5372–5376
44. Ulaganathan M, Pethaiah SS, Rajendran S (2011) Li-ion conduction in PVAc based polymer blend electrolytes for lithium battery applications. *Mater Chem Phys* 129:471–476
45. Wen Z, Itoh T, Ikeda M, Hirata N, Kubo M, Yamamoto O (2000) Characterization of composite electrolytes based on a hyperbranched polymer. *J Power Sources* 90:20–26
46. Wang H, Huang H, Wunder SL (2000) Novel microporous poly(vinylidene fluoride) blend electrolytes for lithium-ion batteries. *J Electrochem Soc* 147:2853–2861
47. Hayamizu K, Aihara Y, Price WSJ (2000) Correlating the NMR self-diffusion and relaxation measurements with ionic conductivity in polymer electrolytes composed of cross-linked poly(ethylene oxide-propylene oxide) doped with $\text{LiN}(\text{SO}_2\text{CF}_3)_2$. *J Chem Phys* 113:4785–4793
48. Park US, Hong YJ, Oh MS (1996) Fluorescence spectroscopy for local viscosity measurements in polyacrylonitrile (PAN)-based polymer. *Electrochim Acta* 41:849–855
49. Aravindan V, Vickraman P, Kumar TP (2008) Polyvinylidene fluoride-hexafluoropropylene (PVdF-HFP)-based composite polymer electrolyte containing $\text{LiPF}_6(\text{CF}_3\text{CF}_2)_3$. *J Non-Cryst Solids* 354:3451–3457
50. Pankove JI (1971) Optical processes in semiconductors. Prentice-Hall, Englewood Cliffs
51. Abdelaziz M, Ghannam MM (2010) Influence of titanium chloride addition on the optical and dielectric properties of PVA films. *Physica B* 405:958–964
52. Maouche N, Nessark B (2011) Cyclic voltammetry and impedance spectroscopy behavior studies of polyterthiophene modified electrode. *Int J Electrochem Sci* 2011:1–5
53. Meher SK, Justin P, Rao GR (2011) Microwave-mediated synthesis for improved morphology and pseudocapacitance performance of nickel oxide. *ACS Appl Mater Inter* 3:2063–2073
54. Appetecchi GB, Croce F, Scrosati B (1997) High-performance electrolyte membranes for plastic lithium batteries. *J Power Sources* 66:77–82
55. Abidin SZZ, Ali AMM, Hassan OH, Yahya MZA (2013) Electrochemical studies on cellulose acetate-LiBOB polymer gel electrolytes. *Int J Electrochem Sci* 8:7320–7326